DOE/PC/94207--T5

Quarterly Progress Report

High Temperature Electrochemical Polishing of H_2S from Coal Gasification Process Streams

Grant DE-FG22-94-PC94207

July 1, 1995 - September 30, 1995

by

Professor Jack Winnick

Georgia Institute of Technology

School of Chemical Engineering

Atlanta, GA 30332-0100

Project Objectives

Coal may be used to generate electrical energy by any of several processes, most of which involve combustion or gasification. Combustion in a coal-fired boiler and power generation using a steam-cycle is the conventional conversion method; however total energy conversion efficiencies for this type of process are only slightly over 30%[1]. Integration of a gas-cycle in the process (combined cycle) may increase the total conversion efficiency to 40%[1]. Conversion processes based on gasification offer efficiencies above 50%[1].

H_2S is the predominant gaseous contaminant in raw coal gas. Coal depending on the type and area of extraction can contain up to 5 wt% sulfur, which is converted to gaseous H_2S during gasification. Problems arise due to the corrosive nature of H_2S on metal components contained in these cycles. Because of this, H_2S concentrations must be reduced to low levels corresponding to certain power applications. For example, an integrated coal gasification-combined cycle (IGCC) process producing electricity from coal at nearly 50% overall efficiency[1] incorporates gas turbines that cannot tolerate H_2S levels above 100 ppm. Coal gasification/Molten Carbonate Fuel-Cell(MCFC) systems, achieving conversion efficiencies around 60%[2], function properly only if H_2S is below 1 ppm.

An advanced process for the separation of hydrogen sulfide (H_2S) from coal gasification product streams through an electrochemical membrane is being developed using funds from this grant. H_2S is removed from the syn-gas stream, split into hydrogen, which enriches the exiting syn-gas, and sulfur, which is condensed from an inert sweep gas stream, Figure 1. The process allows removal of H_2S without cooling the gas stream and with negligible pressure loss through the separator. The process is made economically attractive by the lack of need for a Claus process for sulfur recovery. To this extent the project presents a novel concept for improving utilization of coal for more efficient power generation.

Past experiments using this concept dealt with identifying removal of 1-2% H_2S from gases containing only H_2S in N_2[3], simulated natural gas[4,5], and simulated coal gas[6]. Data

obtained from these experiments resulted in extended studies into electrode kinetics and electrode stability in molten melts[7,8,9]. The most recent experiments evaluated the polishing application (removal of H_2S below 10 ppm) using the Electrochemical Membrane Separator (EMS). H_2S removal efficiencies over 90% were achieved at these stringent conditions of low H_2S concentrations proving the technologies polishing capabilities.

Other goals include optimization of cell materials capable of improving cell performance. Once cell materials are defined, cell experiments determining maximum removal capabilities and current efficiencies will be conducted.

Also, a model theoretically describing the preferred reduction of H_2S, the transport of S^{2-}, and the competing transport of CO_2 will be investigated. The model should identify the maximum current efficiency for H_2S removal, depending on variables such as flow rate, temperature, current application, and the total cell potential.

Introduction

The Electrochemical Membrane Separator (E.M.S.), the focus of experimental work, purges a fuel gas contaminated with H_2S. This is done by reducing the most electro-active species in the gas stream. In this case, H_2S is reduced by the following:

$$H_2S + 2e^- \rightarrow H_2 + S^{2-} \qquad (1)$$

A membrane which contains sulfide ions in a molten salt electrolyte will act to transport the ions across to the anode. If the membrane is impermeable to H_2 diffusion from the cathode side, an inert sweep gas can be used to carry the vaporous oxidized sulfur downstream to be condensed.

$$S^{2-} \rightarrow 1/2\, S_2 + 2e^- \qquad (2)$$

Processes to remove H_2S typically rely on low-to -ambient temperature adsorption, followed by sorbent regeneration and Claus plant treatment for conversion of H_2S to a salable by-product, sulfur. Although effective, this type of removal is very process-intensive as well as energy-inefficient due to low temperature operation. Gasification streams generally range from 500°C - 1000°C, requiring cooling before and reheating after process gas sweetening. Although these technologies have proven capable of meeting H_2S levels required by MCFC, there are several disadvantages inherent to these processes[10,11].

Alternative high temperature methods are presently available, but process drawbacks including morphological changes in catalytic beds[12] or inefficient molten salt sorbent processes[13] negate savings incurred through energy efficient removal temperatures.

An electrochemical membrane separation system for removing H_2S from coal gasification product streams is the subject of this investigation. The high operating temperature, flow-through design, and capability of selective H_2S removal and direct production of elemental

sulfur offered by this process provide several advantages over existing and developmental H_2S removal technologies.

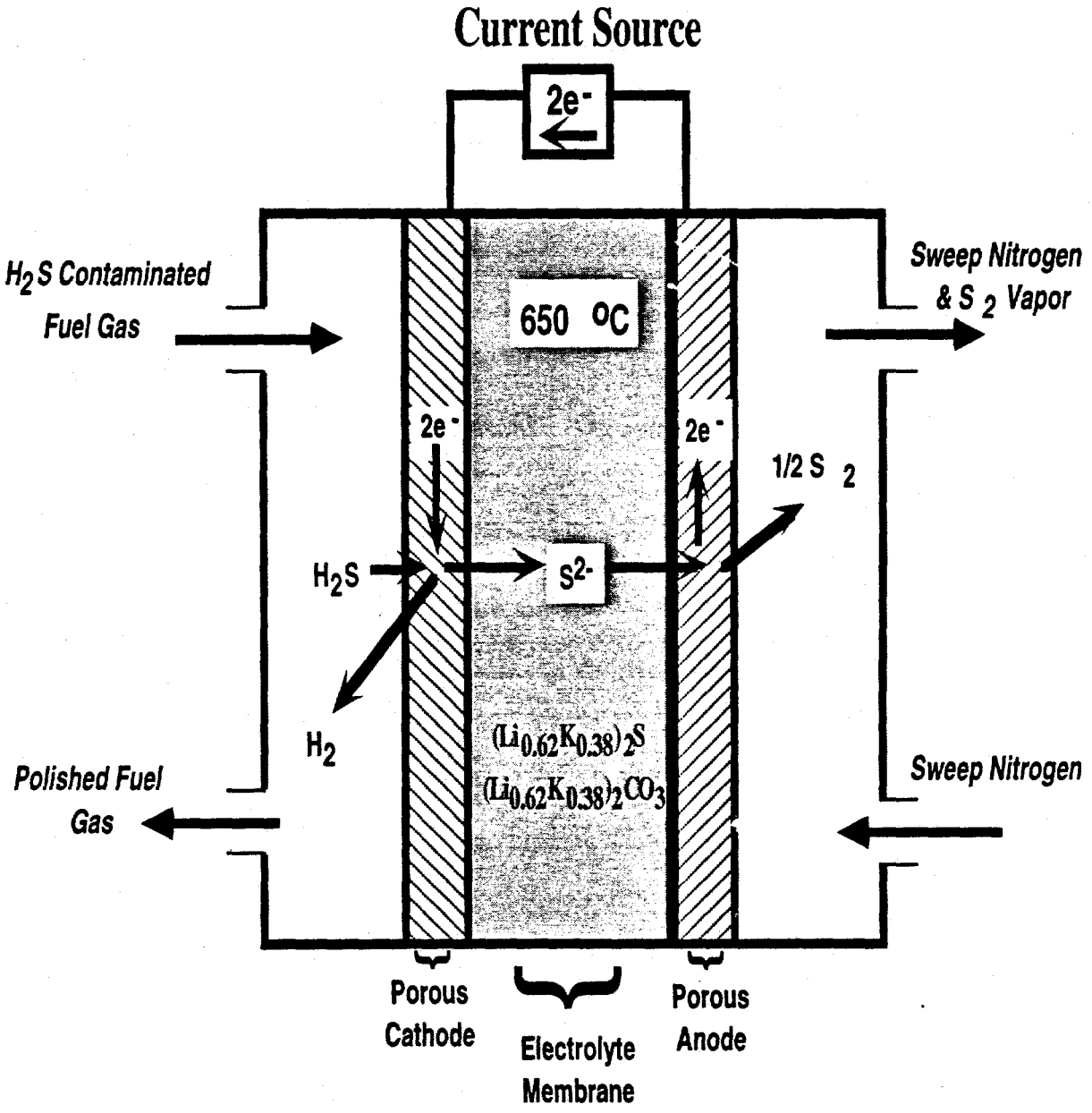

Figure 1. Single-Cell View of the Electrochemical Membrane Separator

Quarterly Research

Electrolyte Management

Electrolyte losses associated with molten carbonate salts is a persistent problem. The mechanism of such losses is not fully understood; CO_2 evolution and reactions with cell materials are possible mechanisms.

Proposed mechanisms for the loss of electrolyte in the E.M.S. are:

1) Material reactions upon process-gas seal formation:

$$2Al + 3/2\ O_2 \rightarrow Al_2O_3 \qquad K = 2.81 \times 10^{78}$$

$$Al_2O_3 + Li_2CO_3 \rightarrow 2LiAlO_2 + CO_2 \qquad K = 154$$

2) Evaporation at the anode due to a deficiency of CO_2:

$$Li_2CO_3 \rightarrow Li_2O + CO_2 \qquad K = 2.51 \times 10^{-5}$$

$$K_2CO_3 \rightarrow K_2O + CO_2 \qquad K = 5.31 \times 10^{-15}$$

3) Evaporation into the surroundings:

$$2Li_2CO_3 + O_2 \rightarrow 2Li_2O_2 + 2CO_2 \qquad K = 3.88 \times 10^{-15}$$

$$2K_2CO_3 + O_2 \rightarrow 2K_2O_2 + 2CO_2 \qquad K = 7.37 \times 10^{-23}$$

with lithium carbonate, comprising 62 mole% electrolyte, being the least stable (larger K).

Quantitative evaporation studies were performed duplicating full-cell conditions[14]. Mechanism (2) & (3) were investigated with evaporation by mechanism (3) entailing the predominant amount of electrolytic losses; 24 hours of exposure evolved on average 30 grams of electrolyte leaving a crystalline residue of Li_2O_2 & Li_2O by:

$$Li_2O_2 \rightarrow Li_2O + 1/2\ O_2 \qquad \Delta G = -41.54\ KJ/mol \quad K = 225$$

After extended real-time experimentation utilizing stainless steel as housing materials, electrolyte diffusion into the housings apparently occurred. This was evidenced during post-mortem analysis; the housings were heated to ~650°C in order to burn-off excess volatiles used for surface sterilization. After thermal cycling crystals appeared on the housing surface; approximately 1.5 grams of the material was recovered for analysis by crystallographic

techniques. X-ray diffraction revealed that the crystals were almost pure lithium carbonate Figure 2. One would expect that potassium carbonate would be apparent as well, in a ratio similar to the molar composition of the electrolyte (62 mole% lithium, 38 mole% potassium).

Mechanism (2) would give a suitable explanation for this phenomenon since diffusion of Li_2O would occur more readily than Li_2CO_3 based on molecular size. This also explains preferential diffusion of lithium species compared to potassium species by comparison of equilibrium constants; dissolution of lithium carbonate is a factor of 10 higher than potassium carbonate.

The conclusion drawn from these findings accentuates the necessity for sealing the electrolyte/housing interface with an electrically as well as chemically inert material of minimum porosity. Continued use of alumina should provide the adequate substrate if the proper technique can be found for inducing a thin, non-porous layer on the stainless steel surface. E-beam deposition as well as sputtering techniques will be attempted in future quarters.

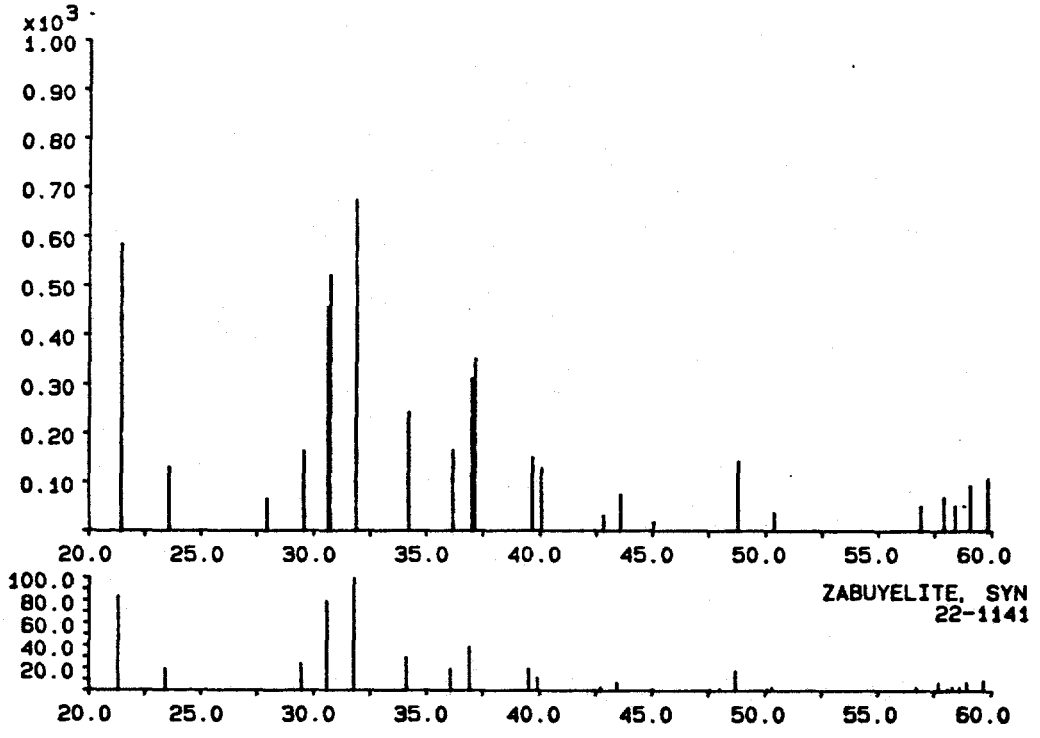

Figure 2. X-ray Diffraction of Crystal Growth on Stainless Steel Housings

Cathode Materials

From results obtained in previous studies, the path to a commercial process is now clear. The primary unresolved components are the cathode and membrane. The cathode must be chemically and mechanically stable in the sulfide/carbonate/hydrogen sulfide environment, and be electronically conductive at 650°C. Lithium-doped NiO has already proven effective in polishing applications; however, the Ni phase transition to liquid $Ni_{3+x}S_2$ when contacting gas with >100 ppm H_2S, requires alternate cathode materials. Co, which converts to Co_8S_9 in-situ, has recently been shown [15], using Scanning Electron Microscopy(S.E.M.), to be morphologically stable in full cell testing with 100 ppm H_2S. The microscopic view revealed adequate porosity and pore size were maintained in the harsh cell environment. Production of cobalt electrodes in the laboratory is ongoing; consistently manufacturing these electrodes with a pore size and arrangement comparable to the Ni electrodes has been accomplished although current attempts have been less successful. Dry pressing the cobalt powder (d_p = 2 microns) with ~ 40 wt% binder (methylethlycellulose) stabilized the metal in disk form to accomplish the burnout and sintering steps. Stress fractures often occur due to the non-uniform release of binder and apparent temperature inequality within the furnace. These concerns involve the physical aspects of dry pressed powders. Non-uniform distribution of binder material incorporated within the cobalt particles creates particle segregation in certain regions; local density gradients due to disproportionate binder distribution effects the final electrode morphology (i.e. pore size, pore distribution, tortuosity, and crystallographic stability). Adjustments dealing with binder content and temperature cycling will be the impetus of future membrane production as well as improvements in dry-pressing of the cobalt-binder system.

Membrane Materials

Several membranes have been utilized in the EMS since its genesis. MCFC tiles used by Weaver[16], sulfided in-situ, resulted in micro-crack development; however MCFC tile technology will be used in scale-up applications of electrochemical separations, due to success in real-time

MCFC. The technology has been refined, but replication in our laboratory is expensive and inefficient for bench-scale testing. Tape-cast membranes of MgO were somewhat more efficient but inconsistent laboratory replication proved detrimental [17]; however, tape casting with zirconia particles still remains a viable option. The most promising membranes for bench-scale experiments have been manufactured zirconia membranes purchased from Zircar Corporation. Polishing of the gasification streams with these membranes confirms their usefulness; however micro-cracks are still evident from S.E.M. analysis[15], Figure 3, and must be controlled. Alternative laboratory-densified membranes with fiber mats replicating the preprocessed membranes from Zircar Corporation are also being investigated. Positive removal results (over 90% H_2S removal) have been obtained from full-cell testing with these membranes [18]; however, more work is needed to improve the manufacturing techniques. Dry pressing zirconia particles admixed with binder has been the most recent attempt to produce a viable membrane material as well as tape-casting sub-micron ZrO_2 particles in a solvent-binder system. Run 23 this quarter utilized a tape-cast membrane which provided a consistent ionic pathway between electrodes as well as segregating process gases from sweep gases.

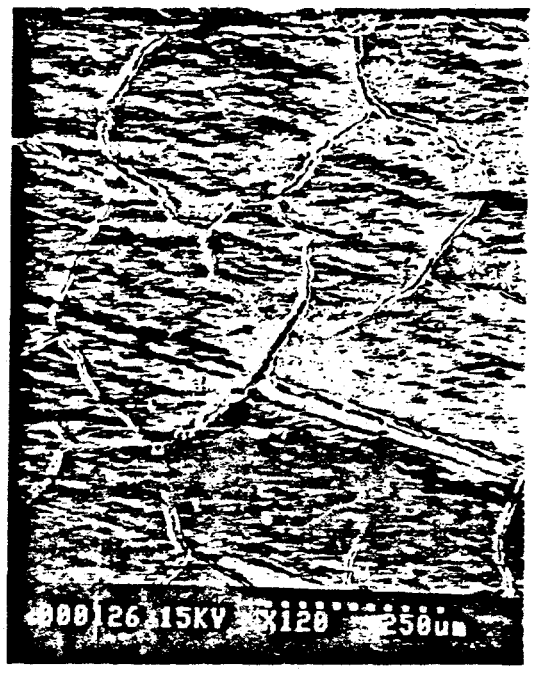

Figure 3. S.E.M. View of a Purchased Zirconia Membrane

Zirconia Cloth-Stabilized Matrices

Continued cell testing will be done utilizing the purchased zirconia membranes along with laboratory-densified zirconia membranes containing zirconia fibers. Laboratory-densified membranes which have proven successful in the past [18] will be tested further. One reason for this is financial. Conventional purchased zirconia membranes cost approximately $ 150.00 per membrane (7.62 cm (3 in) x 7.62 cm (3 in) x 0.063 cm (0.025 in)), compared to $ 10.00 per membrane (7.62 cm (3 in) x 7.62 cm (3 in) x 0.092 cm (0.036 in)) for self-produced membranes.

Laboratory-densified membranes consist of two knit zirconia mats (7.62 cm (3 in) x 7.62 cm (3 in) x 0.0762 cm (0.030 in) purchased from Zircar Corporation. The initial porosity of the mats is approximately 85%. The objective is to fill (rigidize) the knit to a porosity of approximately 65%, which is essential, according to past experiments, in order to operate efficiently[19]. The material used to rigidize the membrane is an aqueous suspension of sub-micron zirconia particles. The combination of mats are submerged in a container of rigidizer, then placed under a vacuum to evacuate the pores. Once pores are relieved of gaseous fillers, the rigidizer infiltrates the pores.

In previous manufacturing, after the infiltration step, the membrane(cloth plus aqueous suspension of sub-micron zirconia particles) was placed on a flat Teflon surface, covered with weighing paper, and constrained from curling by a metal mesh. More recent techniques relied on the wet matrices being placed atop a thin wire bent into a square configuration and attached to a speed controlled rotor; the rotating of the free body should allow a faster more uniformly dry body(matrices) compared to previous techniques.

Once dry, the membrane is analyzed for void fraction and reprocessed if found unacceptable. In the cell, the 65% porous membrane with infiltrated electrolyte prevents cross-over of harmful amounts of hydrogen and allows a low-resistance path for sulfide diffusion and migration. In order to reach such porosity, the method of rigidization must be performed several times, each reducing the porosity by approximately 10%. Every cycle requires drying, placing

mechanical stress on the membrane. The fabricated membrane meeting the 65 % porosity performed adequately in full- cell testing[18].

Thus far improvements in laboratory-densified manufacturing techniques consist of: i) Adding zirconia rigidizer into a knit-zirconia matrix under an extended vacuum (>5 min.). This drastically decreases porosity , reducing the number of steps required to fabricate the membrane. ii) Suspending the mat during drying to increase diffusion since both faces of the mat are exposed, decreasing solvent diffusion distance and iii) vertically rotating the suspended body to uniformly distribute the suspension of zirconia particles throughout the membrane.

Preliminary manufacturing using the rotary dryer failed due to handling problems; Figure 4 reveals an S.E.M. view of membrane cracks connected to these problems. Improvements in the process between steps i and ii are being handled with a more efficient rotor frame, stabilizing the cloth mat prior to the infiltration of the zirconia particles therefore creating a more desirable transition from the vacuum chamber to the rotary drying stage. Processing of membranes with this technique will continue.

Figure 4. S.E.M. View of a Self-Fabricated Zirconia-Cloth Membrane

Dry Pressing

Dry pressing of sub-micron zirconia particles with a percentage of binding material corresponding to a desired porosity has been attempted. Stages in dry pressing include i) the filling of a circular 3 inch diameter carbon steel die with the zirconia particle binder mixture, ii) compacting and shaping of the zirconia binder admixture, and iii) ejection of the pressed disk. Pressing can be accomplished by uni-axial pressing Figure 5a or isostatic pressing Figure 5b. Uni-axial pressing was the technique of choice for initial compression experiments due to ease and availability.

In dry-pressing , pressure produced by moving the die punches compacts the zirconia-binder powder mixture into a cohesive disk with a certain shape and micro-structure according to the extent of applied pressure and binder content. Generally pressures range from 10 - 200 MPa although above 10 MPa rate of densification decreases rapidly; binder content is between 2 and 12 vol% [20]. Dry-pressing of the zirconia-methocel system was accomplished with a pressure of 20 MPa and a binder content of ~ 50 vol%. A high membrane porosity necessitates a higher than normal binder content although inherent problems in binder burnout are inevitable.

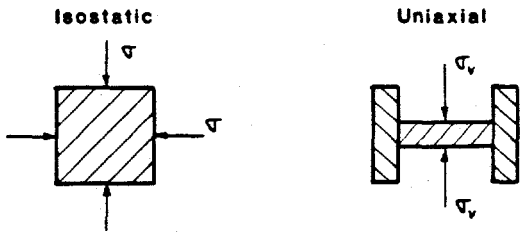

Figure 5 Dry-Pressing with an a) Isostatic Stress Loading and b) Uni-axial Stress Loading

Initial attempts at membrane manufacture by dry-pressing showed promise. Figure 6, an S.E.M. view of the sintered dry-pressed zirconia membrane, reveals an acceptable membrane surface and pore distribution; membrane porosity was ~ 60 % with an average pore size of 1 micron. Work must continue on obtaining a more uniform membrane surface creating parallelism between membrane, electrode, and housing materials as well as alleviating stress fractures during binder burnout and sintering which can lead to cracks. Also reduction in membrane thickness must be addressed in order for the dry-pressed membranes to be a viable options for E.M.S. bench-scale experiments; three experiments yielded a membrane of thickness ~ 0.2 cm. Previous membranes utilized successfully in the E.M.S. removal system had a thickness of ~ 0.5 mm.

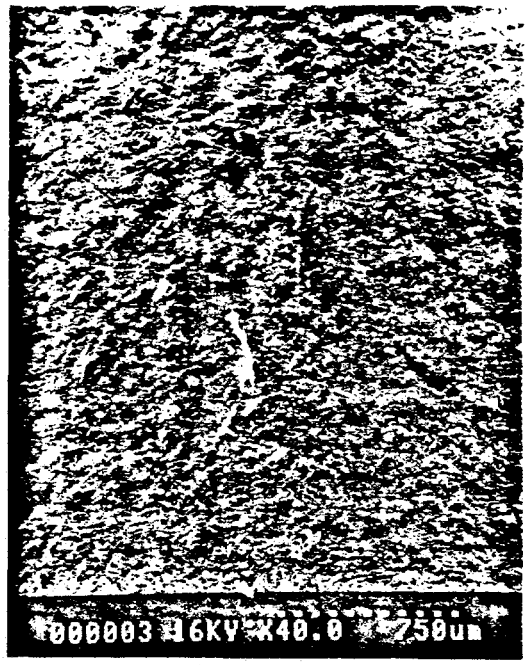

Figure 6. S.E.M view of a Dry-Pressed Membrane

Tape casting

Tape casting is the process of forming a film of controlled thickness under a blade onto a supported substrate. Tape-casting provides a smooth membrane surface as well as a thin (0.01 - 1 mm), flat, uniform, and somewhat compressible membrane [20]. Membranes produced by dry-pressing and extrusion have a less smooth surface below 2 mm in thickness, consist of breakage, non-uniform density, and a non-parallelism between surfaces can be a problem; therefore tape cast membranes if manufactured properly could produce viable membranes for the E.M.S. system, shown in Figure 7. Tape-cast membrane stability throughout the duration of run 23 shows strong support for continued casting efforts.

Tape-casting can be performed continuously or as a batch process. Industrial applications utilize the high volume capacity from continuous casting for multilayer ceramic electronic packaging, multilayer capacitors, piezoelectric devices, thick and thin film insulators, and catalyst supports[20]. Low volume bench-scale requirements (i.e. electrochemical matrices) are ideal for batch production. Examples of batch components used industrially and on our bench-scale membranes are given in Table I and II respectively.

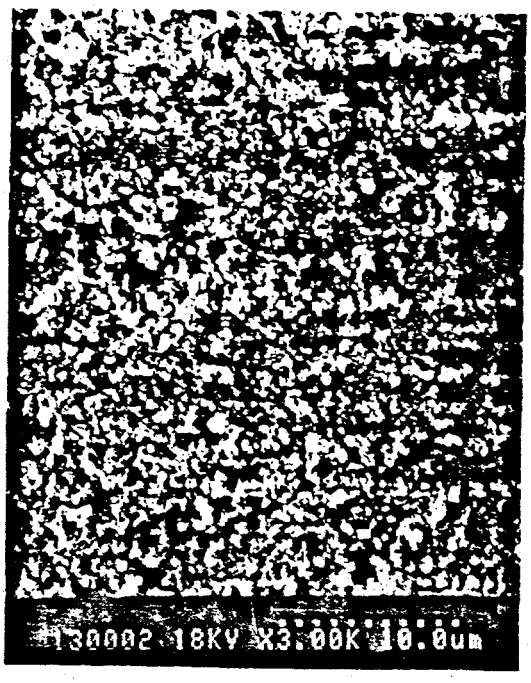

Figure 7. S.E.M. of Tape-Cast Membrane for Bench-scale Experimentation

Table I. Examples of Compositions of Tape-Casting Slurries[20] (Industrial)

Component	Alumina Tape	Comp. (vol%)	Titanate tape	Comp. (vol%)
Ceramic powder	Alumina powder*	27	Titanate powder*	28
Liquid system	Trichlorethylene	42	Methylethyl ketone	33
	Ethanol	16	Ethanol	16
Deflocculant dispersant	Menhaden fish oil	1.8	Menhaden fish oil	1.7
Binder	Polyvinyl butyral	4.4	Acrylic	6.7
Plasticizer	Polyethylene glycol	4.8	Polyethylene glycol	6.7
	Octyl phthalate	4.0	Butyl benzyl phthalate	6.7
Surfactant			Cyclohexanone	1.2

* < 5μm, includes sintering aids, grain growth inhibitor

Table II. Example of Composition of Tape-Casting Slurry (Bench-Scale)

Component	Zirconia Tape	Comp. (vol%)
Ceramic powder	Zirconia powder*	16.3
Liquid system	Toluene	47.9
	Denatured Ethyl alcohol	13.2
Deflocculant dispersant	M-111X	4.5
Binder	Vinyl	8.9*
Plasticizer	Unknown	4.6*
Surfactant	Unknown	4.6*

* compositions are a best guess from characteristic values given by metoramic sciences, inc., see Table IV

Borosilicate membranes

Alternate matrix materials also have been investigated including microporous glass membranes with porosities of 0.2 and 0.02 microns, shown in Figure 8 and a thickness of 60 microns exceeding the probable limit of the bench-scale E.M.S. set-up provisions; thus far, these membranes have shown chemical instabilities with the electrolytic melt. Several experiments to illuminate the chemical stability of these membranes in the molten salt electrolytic melt showed

a trend of membrane dissolution throughout the melt. Without a stable matrices to entrain the electrolyte, leakage will occur reducing the ionic pathway between electrodes which is detrimental to E.M.S. performance. Future tests with these membranes are not scheduled.

Sol-Gel membranes

Testing commenced with SiO_2 Sol-Gel membranes with an engineered pore structure. Chemical testing proved detrimental to the membrane morphology similar to the boro-silicate membranes. The mechanism for SiO_2 dissolution is unknown. Future chemical testing should provide evidence of Sol-Gel membrane usefulness for real-time experiments. An advantage of these membranes involves the ability to manipulated pore structure providing a better ionic pathway as well as electrolytic distribution throughout system components.

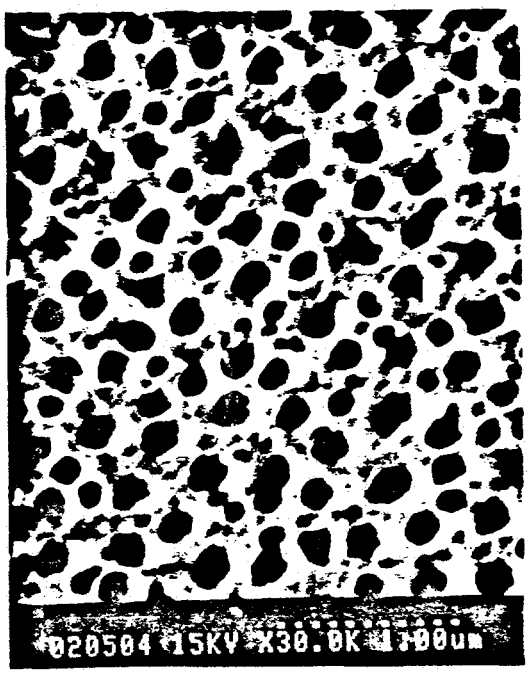

Figure 8. S.E.M. View of a Borosilicate Membrane

Membrane Thickness

Once effective membranes have been developed, other variables such as thickness of the membrane will be investigated in high-flow rate experiments in order to lower the resistance to sulfide migration. The rate of mass transport corresponding to sulfide migration through the membrane is given by:

$$i = \frac{nFD\ (C_c - C_a)}{\delta} \qquad (3)$$

where n is the charge number, F is Faraday's constant, D is diffusion coefficient, δ is the membrane thickness, and C is the concentration of sulfide species at the cathode and anode. At high process-gas flow rates, mass transfer from the gas is equivalent to the limit of diffusion through the membrane, given by:

$$i_l = \frac{nFD\,C_c}{\delta} \qquad (4)$$

The limiting current is a measure of the maximum rate at which sulfide can be transported through the membrane, and occurs when $C_a = 0$. Equation (4) reveals that a thinner membrane creates a higher limiting current for the transport of sulfide. This is extremely important at high flow rates to insure diffusion from the bulk process-gas is the only limiting factor.

Optimization of membrane thickness and porosity will be investigated at high flow rates during full-cell testing using a singular laboratory-densified membrane, thickness ~0.38 mm (0.015 in) as well as tape cast and dry-pressed membranes discussed earlier.

Quarterly Summary

Membrane manufacturing coupled with full-cell experimentation was the primary focus this quarter. A tape-casted zirconia membrane was developed and utilized in a full-cell experiment. Table III gives an outline of the membrane material as well as other components used for the experiment.

One full-cell experiment (run 23) served a three-fold purpose: 1) testing the electrochemical membrane separators ability to concentrate CO_2; 2) testing the electrochemical membrane separators ability to remove H_2S; and 3) testing modifications of the experimental apparatus.

Table III. Experimental Components

Run	Temp. ^oC	Cathode	Anode	Membrane	Housings	Electrolyte
23	650	Lithiated NiO	Lithiated NiO	Tape-cast (ZrO_2)	Stainless Steel (316)	$(Li_{0.62}K_{0.38})_2CO_3$

Run #23

Five ZrO_2 tape-cast membranes were combined for use in the E.M.S. system. The slurry to produce these membranes in a batch-wise process consisted of 20 grams ZrO_2 powder (d_p ~ 0.2 μm) mixed with 14.8 grams of a binder-solvent system (B-73305, characteristics of which are given in Table IV), coupled with 0.1 grams of surfactant/dispersant (M-1114). Mixture of the ceramic, binder-solvent system is based on the desired membrane characteristics; optimal porosity is in the 50 to 70% range with pore diameters of 0.1 microns.

Table IV. Characteristics of the Metoramic Science Binder-Solvent System B-73305

Resin Type	Vinyl
Typical Composition (wt%)	61.3 Toluene 15.3 Denatured ethyl alcohol 23.4 Other additives: polymer, surfactants, plasticizers, adhesion, and porosity modifiers
Typical Properties	Binder solids 22.3 wt% Binder Viscosity 550 cps Binder Specific Gravity 0.88 Binder Solids Specific Gravity 1.0 Wt per Gallon 7.33 lbs. (3.33 kg)
Appearance	Clear to slightly hazy-yellow solution

The ceramic loading into the binder-solvent system necessary for obtaining a ceramic matrices of 50% porosity is calculated as follows:

$$\text{Grams of B73305} = \left(\frac{\text{grams of } ZrO_2}{\text{density of } ZrO_2 \left(\frac{\text{grams}}{\text{cm}^3} \right)} \right) \times \left(\frac{\text{density of binder solids} \left(\frac{\text{grams}}{\text{cm}^3} \right)}{\text{wt\% binder solids} \left(\frac{\text{grams of binder solids}}{\text{grams total}} \right)} \right) \quad (5)$$

Five membranes of 50% porosity were successfully manufactured in a batch-wise process. The dimensions of each membrane are as follows in Table V:

Table V. Tape-cast Membrane Dimensions

Membrane	Weight (grams)	Area (cm x cm)	Thickness (mm)
1	1.68	5.08 x 5.08	0.24
2	1.73	5.08 x 5.08	0.25
3	1.69	5.08 x 5.08	0.25
4	1.56	5.08 x 5.08	0.24
5	1.47	5.08 x 5.08	0.22

The 4.1 grams of electrolyte needed to saturate the combination ceramic membranes was pressed uni-axially into a 3.81 cm diameter disk at 5 MPa prior to cell assembly.

Porous cathode and anode Ni electrodes were obtained from Energy Research Corporation. Both electrodes were lithiated then oxidized at 650 C. Since NiO was used as a cathode material H_2S levels over 50 ppmv could not be applied to the cell due to the phase transition previously evidenced from solid-conductive NiO to the molten-conductive $Ni_{3+x}S_2$. Housing materials consisted of 316 stainless steel with a pressed aluminum disk as process-gas seals.

Upon full-cell start-up the initial temperature was set at 150 ^oC. Binder-burnout was evidenced by smoke and organics in the exhaust. Cathode and anode gas flow rates were 290 cc/min N_2 and 179 cc/min N_2 respectively. Temperature was increased in 10 ^oC intervals, starting from 150 ^oC, as binder volatiles dissipated. Binder volatiles were not apparent after holding the temperature at ~ 470 C (just below the electrolytic melting point of 490 C) for 12 hours. A temperature increase to 590 C resulted in electrolytic melting coupled with total process-gas seal development (i.e. volumetric flow in = volumetric flow out). Cathodic flow was adjusted to 211 cc/min; 108 cc/min was comprised of fuel gas (7.9% CO_2, 11% CO, 14% H_2, and 5.4% H_2O after water-gas shift) and the remaining 136 cc/min of N_2. The anodic inlet gas consisted of 118 cc/min N_2 and 25 cc/min CO_2.

Evaluation of theoretical CO_2 removal from the process-gas (cathode-gas) and anode CO_2 evolution with applied current was the first test conducted on the Electrochemical Membrane Separator (E.M.S.) full-cell run; percentage of CO_2 removal/evolution compared to the theoretical value determines system permanence. Application of 100 mA to the cell caused process-gas CO_2 levels to decrease by 100% of the theoretical value which is necessary before H_2S application. Internal resistance was measured by current interrupt and found to be ~ 3Ω; an acceptable value is 1Ω. A current step method was performed in order to determine CO_2 removal, Figure 9, CO_2 evolution, Figure 10, as well as the potential profile, Figure 11 at varying currents. H_2S addition to the cell occurred once cell stability was proven.

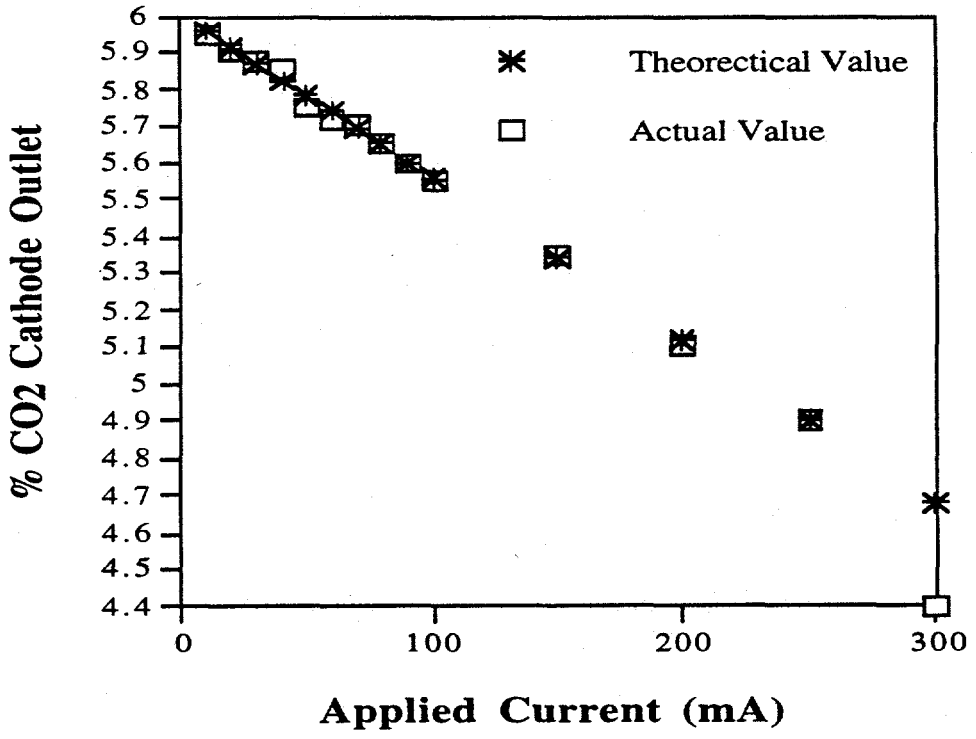

Figure 9. Cathode CO2 level vs. Applied Current

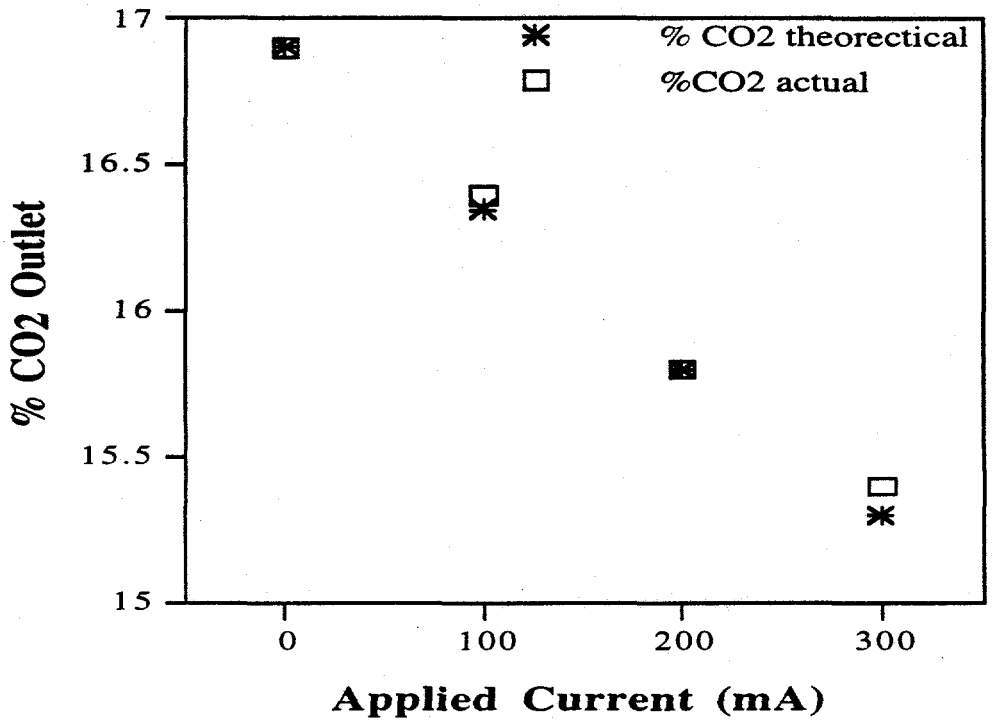

Figure 10. Anode CO_2 Level vs. Applied Current

Upon addition of H_2S, process gas equilibrated to 8.29% CO_2, 10.57% CO, 5.05% H_2O, 14.36% H_2, 24 ppmv H_2S, 1 ppmv COS. The molten-electrolyte - process-gas equilibrium given by:

$$(Li_{0.68}K_{0.32})_2CO_3 + H_2S \Leftrightarrow (Li_{0.68}K_{0.32})_2S + CO_2 + H_2O \qquad (6)$$

creates a conversion of carbonate ions to sulfide ions dependent on the partial pressure of H_2S above the electrolyte; equilibrium electrolyte content consisted of 99.84 mol% $(Li_{0.68}K_{0.32})_2CO_3$, 0.16 mol% $(Li_{0.68}K_{0.32})_2S$.

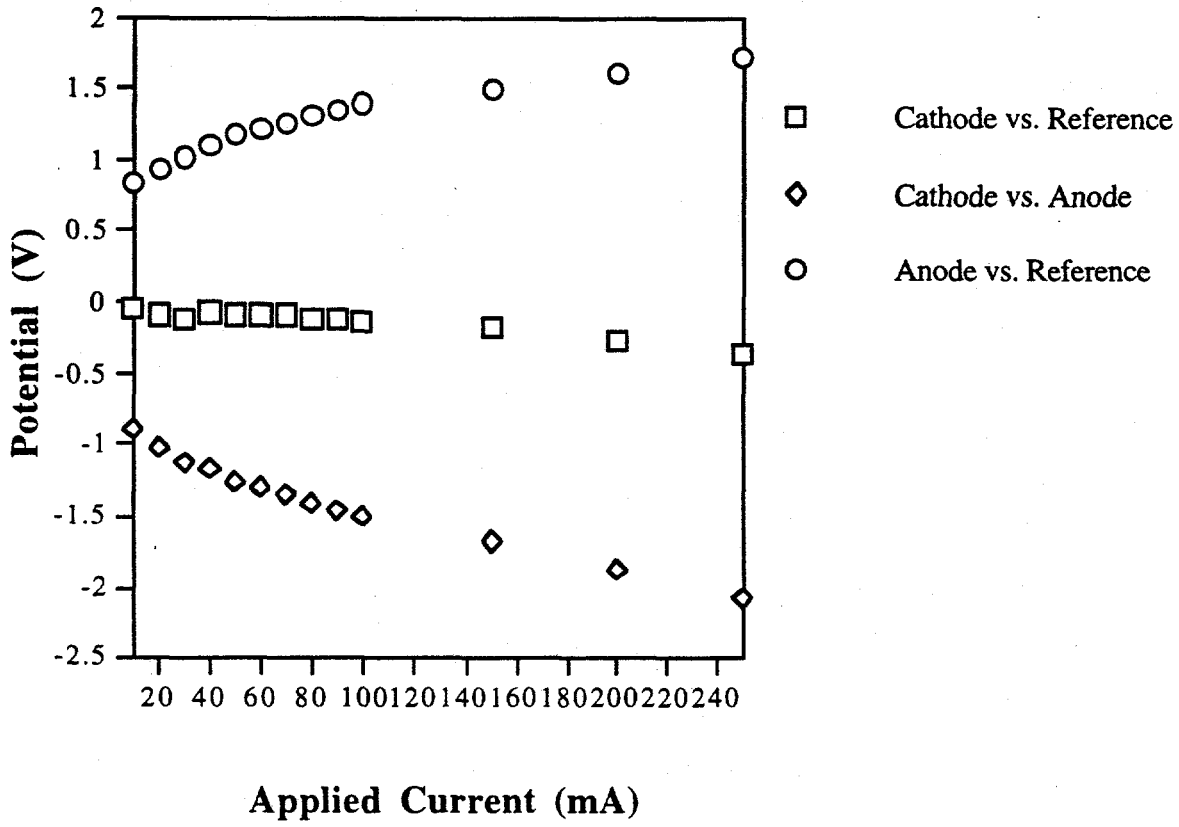

Figure 11. Run 23 Carbonate Transport: Total Cell Potentials vs. Applied Current

Limiting current density analysis within the E.M.S. system shows that the gas-phase limiting current density was 0.2762 mA/cm^2 while the membrane limiting current density was 0.5865 mA/cm^2. This reveals the expedience of ionic transport through the membrane which is two times greater than gas-phase diffusion. Cathode and anode electrode areas were both 11.40 cm^2; therefore the maximum applicable current to the cell for H_2S removal was 3.2 mA before exceeding the limiting current based on bulk-gas diffusion of H_2S. Stoichiometric current needed to remove 25 ppmv H_2S down to 2.5 ppmv H_2S is 0.51 mA.

Problems occurred soon after introduction of H_2S to the E.M.S. system due to the high concentration initially sent into the system. Approximately 170 ppmv H_2S was released into the

system which eventually proved detrimental by creating the proper conditions at the (Li)NiO electrode surface for a phase transition to $Ni_{3+x}S_2$. Post-Mortem analysis revealed a decrease in electrode diameter from 3.81 cm to 2.4 cm. This can be explained from the previous mentioned phase transition creating a molten conductive phase, $Ni_{3+x}S_2$, causing pore structure collapse; therefore, little area for electron transfer reactions. X-ray diffraction of the cathode revealed this assumption to be true, Figure 12, by matching a fraction of the electrode to heazlewoodite (Ni_3S_2).

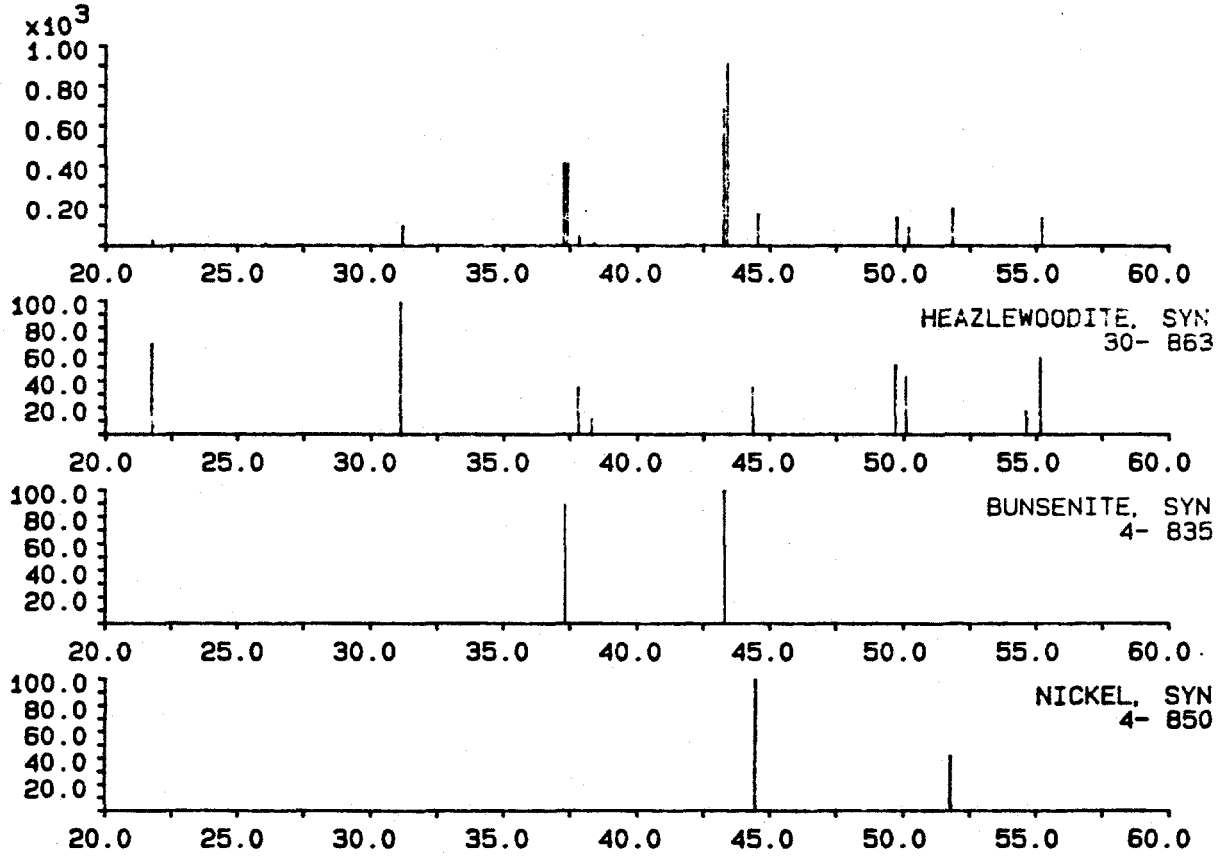

Figure 12. X-ray Diffraction Pattern of Run 23 Cathode Material

Upon equilibration of the electrolyte and process-gas species (H_2S inlet = H_2S outlet at varying flow rates) current was applied to the cell to test H_2S removal capabilities. Figure 13 shows inlet and outlet H_2S levels at varying currents. Although effective H_2S removal did not occur, Figure 13 does reveal at currents above the limiting H_2S current of 3.2 mA an appreciable increase in outlet H_2S. This is a result of the parasitic reaction, CO_2 removal, taking precedence over H_2S removal due to the concentration advantage (on the order of 10^3 more CO_2 molecules than H_2S molecules). Figure 14 shows cell potentials with applied current. Again evidence of Carbonate transport can be ascertained from comparing the cell potentials for H_2S removal and the Nernst potential for carbonate transport; potentials in the proximity of the limiting current (3.2 mA) are in the range for carbonate transport.

The problem must be associated with pore structure collapse upon cathode phase transition making diffusion of species to the electrode-electrolyte interface difficult; therefore creating a more negative total cell potential by increasing the mass transfer overpotential.

Future experiments will be conducted with the proper electrode phase (Li)Ni present at the cathode to insure correct cell operation.

Tape-cast membrane materials will continue to be used due to there stability throughout the duration of Run #23.

Run #23 was shut-down after 312 hours(13 days) of operation.

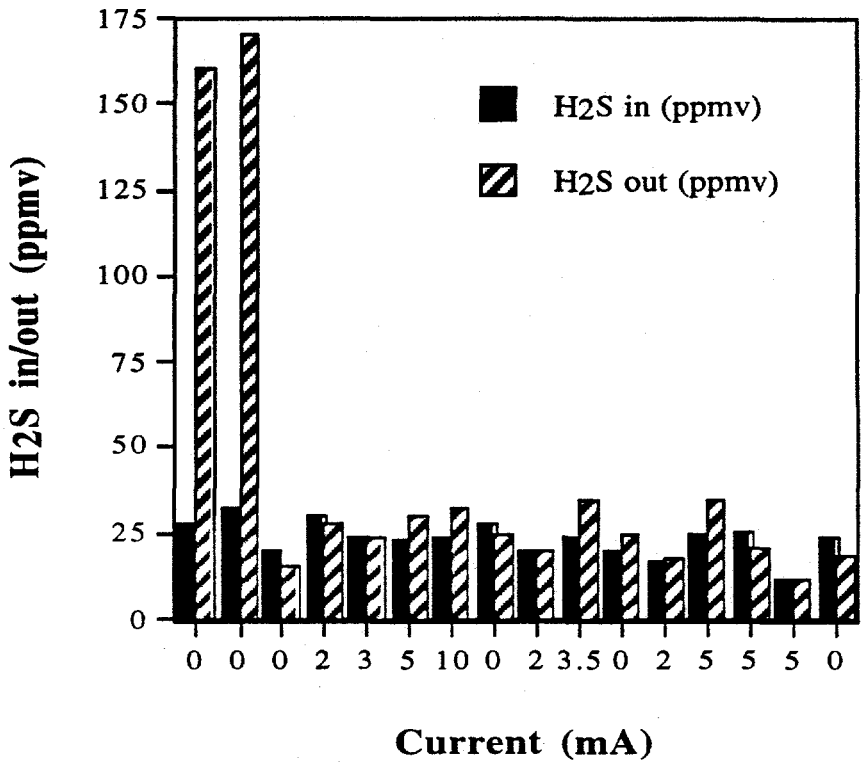

Figure 13. H_2S inlet/outlet vs. Applied Current

Conclusion

The Fossil Energy Advanced Research Program requires high temperature separations to remove environmental contaminants from post-combustion flue gases as well as pre-combustion process gases. This project is aimed at the latter: the removal of hydrogen sulfide from coal gas at gasifier temperatures. This development would enable a simplification of the entire gasification scheme by permitting a one-step removal of hydrogen sulfide and production of elemental sulfur. Energy savings accrue due to the high temperature processing.

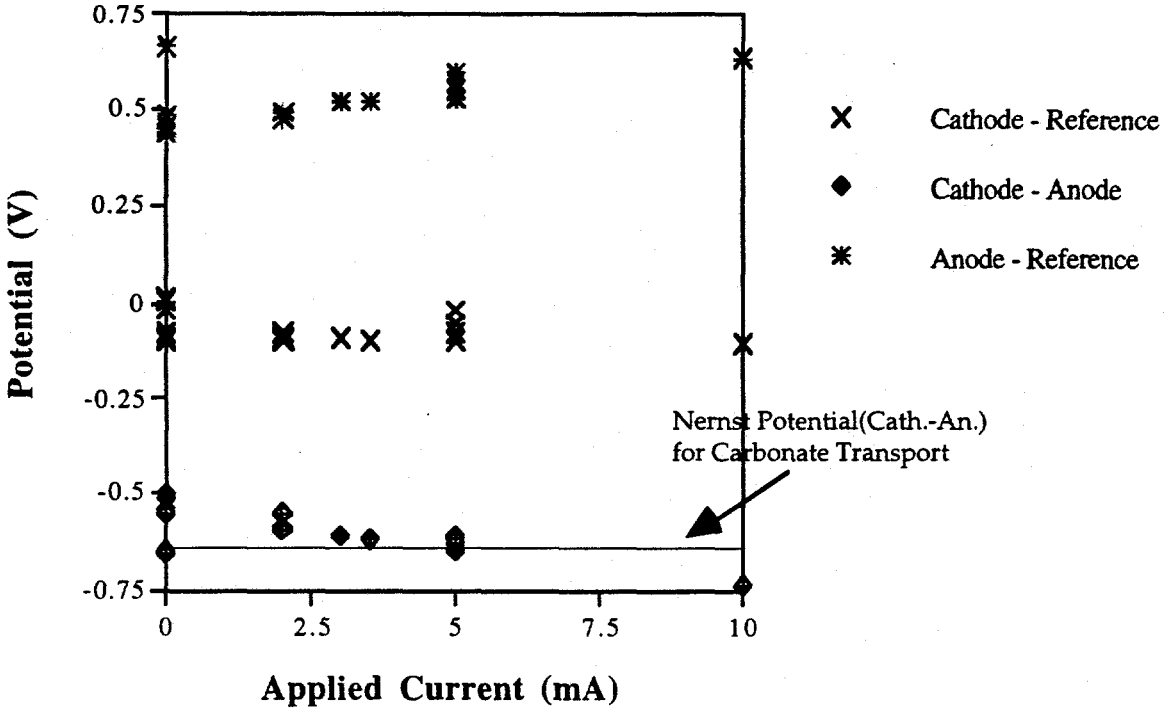

Figure 14. Cell Potentials vs. Applied Current for H_2S Removal

The DOE programs relating to gasification for power production have as their goal the more efficient, clean paths toward affordable energy from coal. Gas clean-up accounts for nearly one-third of the cost of this conversion. Simplification and economization will benefit the entire effort.

Project Output

Current experiments are based on improving selective removal from low initial H_2S concentrations (100 ppm and 20 ppm H_2S). High flow rate effects, membrane stability and selectivity, and electrode morphology characterizes present studies, with recent results showing over 90% H_2S removal with applied current.

Experimental results presented are based on two experiments with initial H_2S concentrations of 100 ppm and 20 ppm. To represent probable industrial conditions, variables such as flow rates, selectivity of the membranes, and process-gas seals, were of primary concern in these experiments. Maximum removals of H_2S are reported on a zero current basis, thus compensating for any chemical scrubbing effects of the non-equilibrium electrolyte species in the membrane. Percent H_2S removal with applied current exceeded 80% and in some cases reached 90%, given by:

$$\%H_2S\ \text{Removal} = \frac{\left(\text{Outlet } H_2S_{\text{zero current}} - \text{Outlet } H_2S_{I_{\text{applied}}}\right)}{\left(\text{Outlet } H_2S_{\text{zero current}}\right)} \times 100 \qquad (7)$$

Cell housing materials used for both experiments were a machineable ceramic (MACOR). Cathode and anode electrodes consisted of Ni, oxidized in situ to form NiO. Process-gas seals developed, in-situ, by placing aluminum foil gaskets on both sides of the electrolyte filled membrane. Al oxidation initially forms Al_2O_3 which on reaction with Li, contained in the electrolyte, forms $LiAlO_2$.

The membrane for the 100 ppm experiment, used two tapes of MgO and one mat of zirconia cloth. Acrylic binders used in the MgO tapes (Metoramics K565-4 binder system) were burned out under an O_2 atmosphere at 350°C and the $(Li_{0.62}K_{0.38})_2CO_3$ eutectic-composition electrolyte was added with the cell at run temperature. Inlet gases were passed through a stainless steel shift reactor, allowing them to equilibrate before passing through the cell. Gas compositions at 973K after the shift reactor were 14.3% CO_2, 50.8% CO, 4.8% H_2O, 30.1% H_2, and 100 ppm H_2S.

H_2S removal vs. applied current, with a cathodic flow rate of 88 cc/min., is presented in Figure 15. H_2S removals of 90% were achieved with H_2S current efficiencies of 5%.

The membrane for 20 ppm experiments was purchased from Zircar Corporation, consisting of yttria-stabilized zirconia in a rigid form at 66% porosity. The advantages of these

membranes are consistently uniform porosities and no warping. A cold pressed disk of the Li/K eutectic carbonate electrolyte, placed between the cathode housing and the Zircar membrane, provided a stable start-up configuration. Inlet gases equilibrated to 5.8% CO_2, 25.6% CO, 6.7% H_2O, and 65.3% H_2, after the water-gas shift reactor. The electrolyte sulfide concentration equilibrated in-situ to 0.11 mole%.

Temperature remained constant (650°C) while flow rates varied from 170 cc/min. to 814 cc/min. H_2S removal at all flow rates exceeded 80% with applied current as shown in Figure 16; Current efficiencies were ~ 35%.

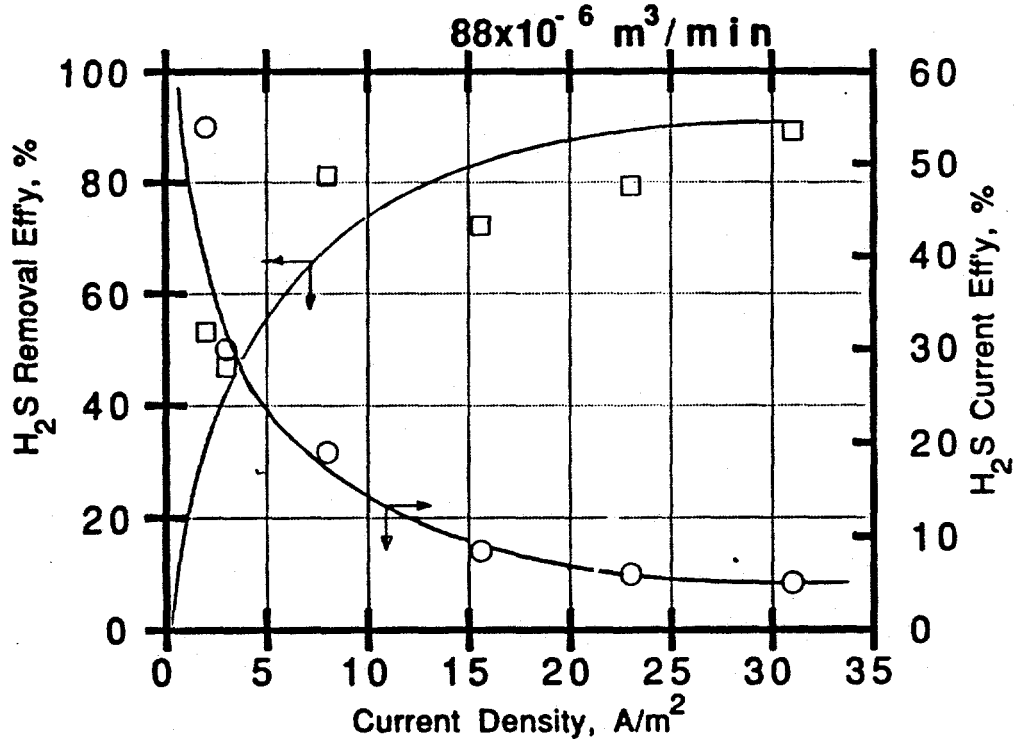

Figure 15. H_2S Current and Removal Efficiency vs. Current Density; 100 ppm inlet H_2S Cathodic Flow Rate = 88 cc/min

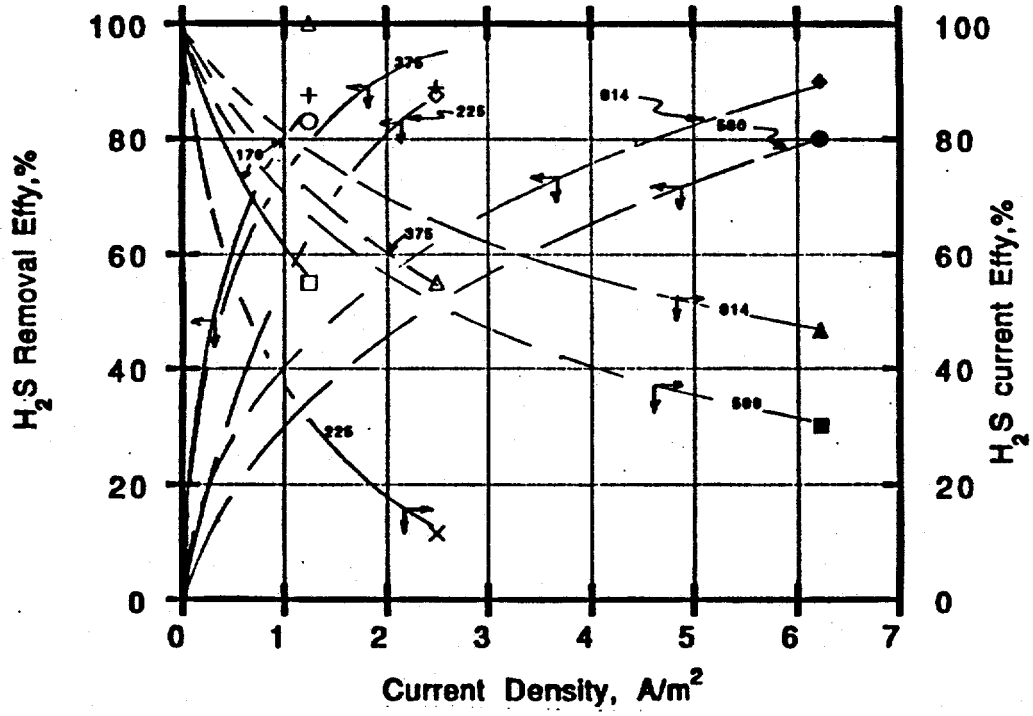

Figure 16. H_2S Current and Removal Efficiency vs. Current Density; 20 ppm inlet H_2S

Parametric values are in cc/min

References

1. U.S. Dept of Energy, DOE/METC 87/0255, DE87006493, Oct., 1987.
2. Skerret, P.J., "Fuel Cell Update", *Popular Science*, 89-91, 120-1, June, 1993.
3. Lim, H.S. and Winnick, J., *J. Electrochem. Soc.*, **131, 562-8** (1984).
4. Alexander, S., and Winnick, J., *1990 AIcHE Annual Meeting*, Chicago, IL., 1990.
5. Alexander, S., and Winnick, J., *Sep'n Sci. and Tech.*, **25**, 2057-72 (1990).
6. Weaver, D., and Winnick, J., *J. Electrochem. Soc.*, **134**, 2451-58 (1987).
7. Weaver, D., and Winnick, J., *J. Electrochem. Soc.*, **138**, 1626-37 (1991).
8. Banks, E., and Winnick, J., *J. Appl. Electrochem.*, **16**, 583-90 (1986).
9. White, K.A., and Winnick, J., *Electrochim. Acta*, **30**, 511-516 (1985).
10. EPRIEM-1333, *Assessment of Sulfur Removal Processes for Advanced Fuel Cell Systems, Final Report,* C.F. Braun and Co., Alhambra, CA, Jan., 1980.
11. Vidt, E.J., DOE/METC DE-AC-21-81MC16220, DE82013942, Westinghouse, Dec., 1981.
12. Focht, G.D. et. al., DOE/MC/121166-2163, DE86016041, July, 1986.
13. Lyke, S.E., DOE/MC/19077-1803, DE8500961, Battelle Pacific Northwestern Laboratories, Jan. 1985.
14. Winnick, J., Quarterly Progress Report #13, DOE grant DE-FG-91PC91288.
15. Winnick, J., Quarterly Progress Report #11, DOE grant DE-FG-91PC91288.
16. Weaver, D., and Winnick, J., *J. Electrochem. Soc.*, **139**, 492-498 (1992).
17. Alexander, S., *Ph.D. Thesis*, Georgia Institute of Technology, Atlanta, GA, 1992.
18. Winnick, J., Quarterly Progress Report #6, DOE grant DE-FG-91PC91288.
19. Winnick, J., Quarterly Progress Report #8, DOE grant DE-FG-91PC91288.
20. Reed, James S., Introduction to the Principles of Ceramic Processing, John Wiley & Sons, New York, 1988.